Supporting Information

Electronic Structure Modulation to Enhance Internal Electric Field and Artificial Photosynthesis by Br Introduction in Layered $Bi_xO_yBr_z$

Jingjing Liu[a], *Ruonan Wang*[a, b]*, *Qin Zhong*[a]*

[a] School of Chemistry and Chemical Engineering, Nanjing University of Science and Technology, Nanjing, Jiangsu 210094, PR China

[b] School of Chemical Engineering, Nanjing Forestry University, Nanjing, Jiangsu 210037, PR China

Ruonan Wang. Email: wang__rn@163.com

Qin Zhong. Email: zq304@njust.edu.cn

S1. Preparation of photocatalysts

Materials and reagents: Bismuth nitrate pentahydrate (Bi $(NO_3)_3 \cdot 5H_2O$, AR, 99 %) was purchased from Shanghai Macklin Biochemical Technology Co., Ltd. Potassium bromide (KBr, AR, 99 %), hexadecyl trimethyl ammonium bromide (CTAB, 99 %), PVP (K30), mannitol (AR, 98 %), ethanolamine (AR, 99 %) and triethanolamine (TEOA, AR) were purchased from Aladdin chemical reagent company. Sodium hydroxide (NaOH, AR) and nitric acid (HNO_3, AR) were purchased from Sinopharm Chemical Reagent Co., Ltd. All chemicals and materials were used as received without further purification.

Preparation of Bi_2O_3: Firstly, $Bi(NO_3)_3 \cdot 5H_2O$ (4.8 g) was dissolved into 100 mL of deionized water with stirring for 0.5 h. Thereafter, the pH value of the solution was adjusted to 8.0 using NaOH (10 M) and the as-obtained suspension was ultrasonicated for 1 h. Then, the mixture was stirred overnight, and the precipitate was centrifuged and washed three times with deionized water. Finally, the light-yellow Bi_2O_3 nanobelts were harvested after calcined at 400 °C for 2 h in air.

Preparation of Bi_3O_4Br: 0.15 g PVP (K30) and 0.485 g $Bi(NO_3)_3 \cdot 5H_2O$ were dissolved in 10 mL (0.1 M) mannitol solution, named solution A. In the meantime, 0.119 g KBr was dispersed into 3 mL (0.1 M) mannitol solution, named solution B. Subsequently, solution B was added slowly dropwise to solution A, and stirred for 0.5 h. Then, 2 mL (0.1 M) mannitol and 1.5 mL ethanolamine was added into the above mixture, followed by stirring for another 0.5 h. The above solution was transferred into a 40 mL Teflon-lined autoclave and heated at 160 °C for 12 h. Finally, the product was

washed three times and dried at 60 °C to acquire Bi_3O_4Br nanosheets.

Preparation of $Bi_4O_5Br_2$: 4. 85 g $Bi(NO_3)_3 \cdot 5H_2O$ was dissolved in 10 mL of 20 mM HNO_3 solution and stirred for 10 min, followed by stirring for 3 min in a 70 °C water bath. Subsequently, 20 mL of 9 mM CTAB solution was added and stirred for 2 min. After that, 30 mL of the solution containing 3.6 g NaOH and 7.14 g KBr was added drop by drop into the above suspension with stirring for 10 min. On this basis, the resulting $Bi_4O_5Br_2$ product was obtained after washing with distilled water by centrifugation and drying at 60 °C overnight.

Preparation of BiOBr: BiOBr nanosheets were prepared by a simple solvothermal method. $Bi(NO_3)_3 \cdot 5H_2O$ (0.97 g) was dissolved in 30 mL deionized water and subjected to sonication for 0.5 h, named solution A. Then KBr (0.238 g) was dissolved in 30 mL deionized water and also subjected to sonication for 0.5 h, marked as solution B. The solution B was added into solution A drop by drop and stirred for 1 h. Subsequently, the above solution was transferred into the Teflon-lined stainless-steel autoclave and heated hydrothermally at 160 ℃ for 12 h. Finally, BiOBr was obtained by centrifugation, washing and vacuum drying at 60 °C.

S2. Reaction mechanism for as-prepared $Bi_xO_yBr_z$

As depicted in **S1**, pentahydrate bismuth nitrate ($Bi(NO_3)_3·5H_2O$) and potassium bromide (KBr) were utilized as the sources of bismuth and bromine, respectively, for all $Bi_xO_yBr_z$. The possible reaction mechanism was described as follow.

Bi_2O_3: The synthesis of Bi_2O_3 involved two steps:

Firstly, $Bi(NO_3)_3·5H_2O$ reacted with NaOH, producing bismuth oxide (Bi_2O_3) and sodium nitrate ($NaNO_3$), according to the following reaction:

$$2Bi^{3+} + 6OH^- \rightarrow Bi_2O_3 + 3H_2O \quad (1)$$

Secondly, the precipitate was calcined to enhance the crystallinity of Bi_2O_3.

Bi_3O_4Br: For the synthesis of Bi_3O_4Br, PVP was employed to control the introduction of Br, while mannitol, a polyhydric compound, served as the solvent. Bi^{3+} has three primary bond vacant orbitals and with a lone pair electron in its outermost shell, it can be used as Lewis base to form a 4-or 6-coordination complex. Hence, Bi^{3+} initially engaged in coordination reactions with mannitol to form multi-coordinate complexes. Simultaneously, the ionization of ligands resulted in the generation of H^+ [1]. The detailed reactions proceeded as follows:

$$xBi^{3+} + zH_2O + yM \rightarrow Bi_x(M)_y(OH)_z + zH^+ \quad (1)$$

$$Bi_x(M)_y(OH)_z \rightarrow Bi_x(*M)_y(OH)_z + yH^+ \quad (2)$$

M-mannitol, * indicated dissociation state.

On the basis, Ethanolamine, utilized as an alkaline pH regulator, effectively facilitated the substitution of M by OH^- during the solvent thermal process, thereby promoting the formation of Bi-O-Bi [2]. Meanwhile, the introduction of KBr enabled a selective reaction between Br^- and Bi-O-Bi, leading to the substitution of certain O atoms. Consequently, the synthesis yielded Br-poor Bi_3O_4Br.

$Bi_4O_5Br_2$: In the process of synthesizing $Bi_4O_5Br_2$, precise control over the introduction of Br was achieved through two crucial factors. The first factor involved meticulous adjustment of the molar ratio between the Bi source and Br source, ensuring the desired stoichiometric composition. The second factor entailed fine-tuning the pH value of the

solution, recognizing its significant influence on the reaction between $Bi(NO_3)_3 \cdot 5H_2O$ and KBr, as reported in prominent literature [3, 4]. During this intricate process, bismuth nitrate ($Bi(NO_3)_3$) underwent an initial reaction with water, laying the foundation for subsequent steps in the synthesis:

$$Bi^{3+} + H_2O \rightarrow BiO^+ + 2H^+ \quad (1)$$

In this highly acidic environment, the direct introduction of KBr will lead in an excessive amount of Br being introduced. To address this, a substantial quantity of NaOH was judiciously added to meticulously adjust the pH level, ensuring optimal conditions for effectively regulating the Br content. Specifically, a large quantity of OH^- ions hindered the combination of Br^- with BiO^+, thereby promoting the formation of $Bi_4O_5Br_2$.

$$4BiO^+ + 2Br^- + 2OH^- \rightarrow Bi_4O_5Br_2 + H_2O \quad (2)$$

BiOBr: For BiOBr, the synthesis process also consists of two steps. Firstly, $Bi(NO_3)_3$ reacted with water, which was consistent with $Bi_4O_5Br_2$.

$$Bi^{3+} + H_2O \rightarrow BiO^+ + 2H^+ \quad (1)$$

However, in the absence of OH^- competition, the reaction of Br^- with BiO^+ proceeded comprehensively, resulting in the introduction of a larger quantity of Br. This process was predominantly guided by the following subsequent process:

$$BiO^+ + Br^- \rightarrow BiOBr \quad (2)$$

S3. Photocatalyst Characterization

Structure and morphology characterizations: X-ray diffraction (XRD) test is conducted on a Bruker D2 PHASER system under 36 kV and 30 mA with Cu Kα radiation. The data is collected from 5° to 80° at a scanning rate of 8° min^{-1}. The textures performances of the photocatalysts were measured by N_2 adsorption-desorption apparatus (Micromeritics ASAP 2460). The specific surface area and pore diameter were determined and calculated by the Brunauer-Emmett-Teller (BET) and Barrett-Joyner-Halenda (BJH) methods, respectively. The morphology and elemental distribution of the prepared samples were observed with scanning electron microscopy (SEM, Hitachi S4700) and transmission electronic micrograph (TEM, Tecnai G2 F30). For TEM, the sample was ultrasonically dispersed in ethanol for 10 minutes, and the supernatant was dropped on a copper screen, and dried for characterization. As for SEM, the powder sample is smeared on conducting resin for analysis.

Band structure characterizations: X-ray photoelectron spectroscopy (XPS) tests of the catalysts are performed on a Thermo ESCALAB 250 spectrometer with a mono-chromated Al K-alpha source with a power of 150 W. Ultraviolet-visible diffuse reflectance spectroscopy (UV-vis DRS) are conducted on a Shimadzu UV-2600 spectrophotometer with a wavelength range of 220-800 nm using $BaSO_4$ as the reference.

The band gaps of photocatalysts were obtained by Tauc's equation (**Eqs. 1**):

$$(\alpha h\nu)^{1/n} = A\,(h\nu - E_g) \qquad (1)$$

where "α" was absorption coefficient; "hν" was the incident photon energy; "A" was an energy independent constant; "E_g" was the bandgap energy; "n" was determined by the transfer characteristics of electrons in a semiconductor ("n" was 0.5 and 2 for direct allowed transition and indirect allowed transition, respectively).

Photoelectrochemical characterizations: For EIS, open-circuit potentials, photocurrent and Mott-Schottky characterizations, the working electrode is prepared as follows: A 0.5 mol L^{-1} Na_2SO_4 solution is used as the electrolyte. The working electrode

is prepared as follows: 5 mg catalyst is dissolved in a solution containing 30 μL Nafion and 1 mL ethanol. After ultrasonically scattering for 1 h, the slurry is dip-coated onto an FTO glass (1 cm × 1 cm) and dried at 80 ℃ for 5 h under a vacuum atmosphere. All the experiments are conducted under a 300 W Xe lamp irradiation.

Surface adsorption and activation characterizations: CO_2 pulse chemisorption experiments were conducted on an AutoChem II 2920 apparatus instrument (Micromeritics, America) using 0.05 g photocatalysts. Piror to experiments, He (10 mL min^{-1}) passed through the photocatalysts at 100 ℃ for 30 min to remove surface impurities. Subsequently, CO_2 was pulse adsorbed by photocatalysts for 20 times.

In-situ DRIFTs experiments are performed on a Nicolet IZ10 spectrometer equipped with a Harrick Scientific DRIFT cell. Prior to the test, photocatalysts are pretreated at 100 ℃ under N_2 flow (20 mL min^{-1}) for 60 min and then get the background spectrum. After N_2 flow stops, CO_2 (20 mL min^{-1}) with bubbled H_2O is introduced into the chamber and reacted at dark for 30 min. Then, the light source is turned on to monitor the produced intermediates for another 30 min.

S4. Calculation method of CO production rates

Firstly, 1 mL 0.505 % CO calibrating gas was detected and quantified online by a gas chromatograph, gaining an area ($A_{0.505\ \%\ CO}$). Then, 1 mL produced gas after the photocatalytic reaction was injected into a gas chromatograph and gained another area (A_{CO}). Finally, the CO production rates can be calculated by the following **Eqs. (2)**:

$$Yield_{CO} = \frac{P_{CO} * V_{CO} * n_0 * 0.505\%}{P_0 * A_{0.505\%} * T * m} \qquad \textbf{(2)}$$

where "P_{CO}" was the pressure at the outlet of the reactor; "V_{CO}" was the volume of the reactor; "n_0" was the total number of molecules in 1 mL of gas, which was easily obtained by the formula of $PV = nRT$; "P_0" was standard atmospheric pressure; "T" was the time of reaction; "m" was the dosage of photocatalysts.

S5. Recycle experiments upon BiOBr

Firstly, the cyclic experiments were conducted under the conditions of the normal activity tests as shown in **S1** (60 ℃, 0.6 MPa, 300 W Xe irradiating for 4 h), and 1 mL of the gaseous product was analyzed by gas chromatography after the reaction. Following the initial analysis, the photocatalyst in the reactor was recovered and then reused for another round of photocatalytic CO_2 reduction using the exact same method as before. This procedure was repeated 5 times, with the yield of the detected products recorded for each iteration.

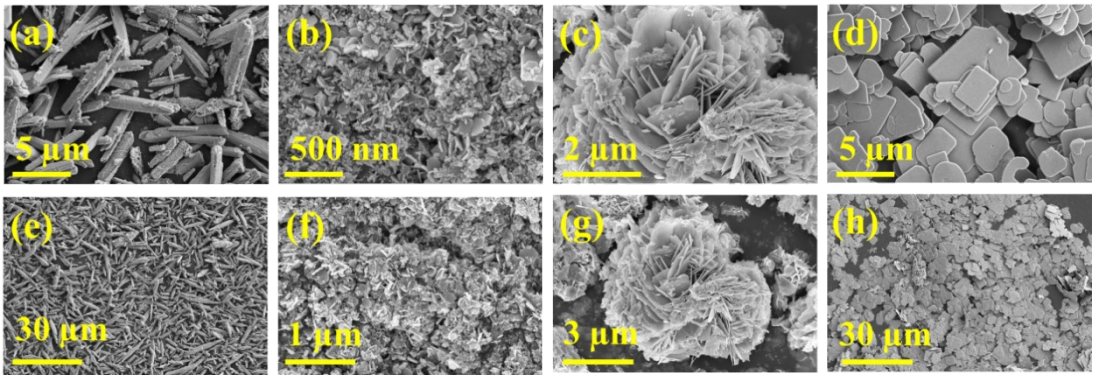

Figure S1. SEM images of (a, e) Bi_2O_3, (b, f) Bi_3O_4Br, (c, g) $Bi_4O_5Br_2$ and (d, h) BiOBr.

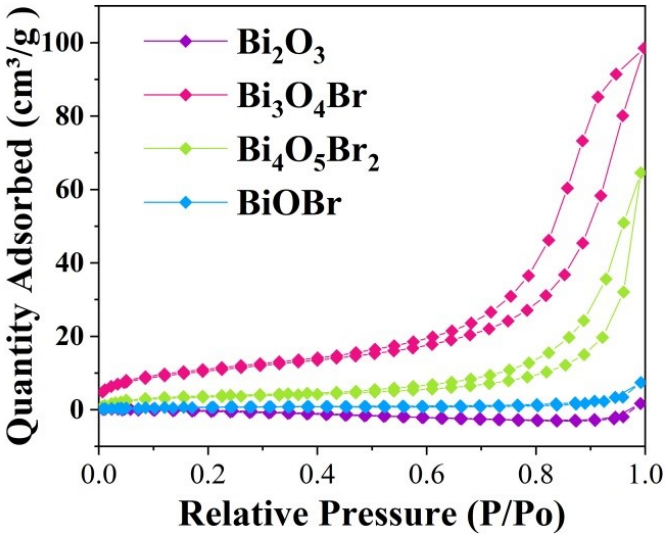

Figure S2. N_2 adsorption-desorption isotherms of the as-prepared $Bi_xO_yBr_z$ materials.

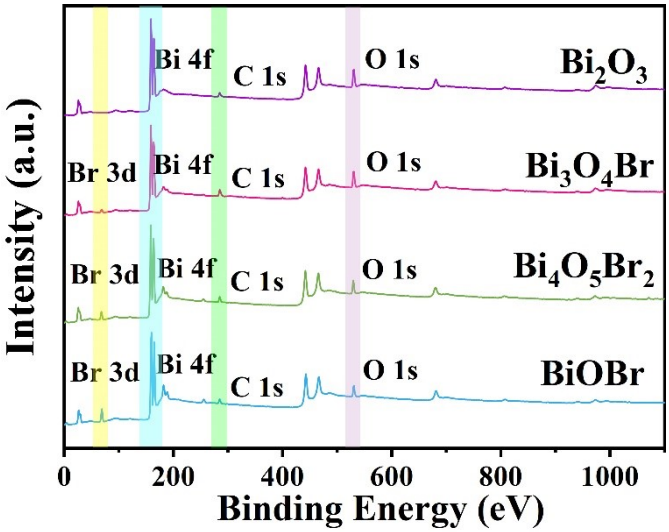

Figure S3. XPS survey spectra of $Bi_xO_yBr_z$.

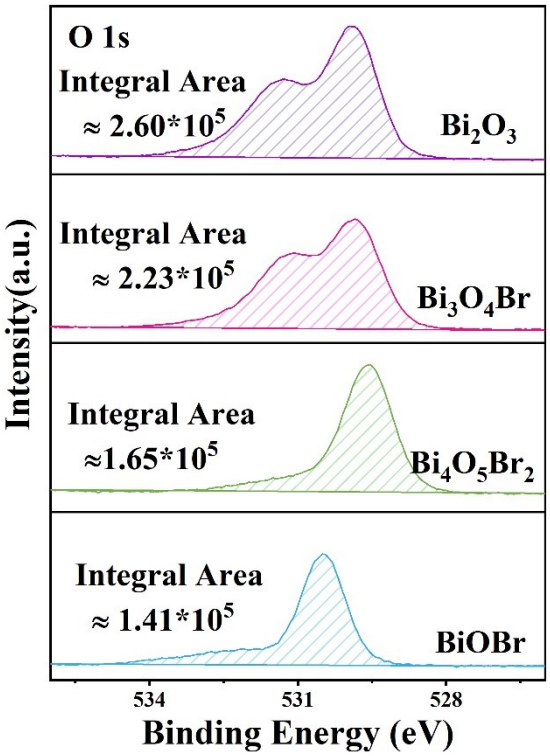

Figure S4. The O 1s XPS spectra for $Bi_xO_yBr_z$.

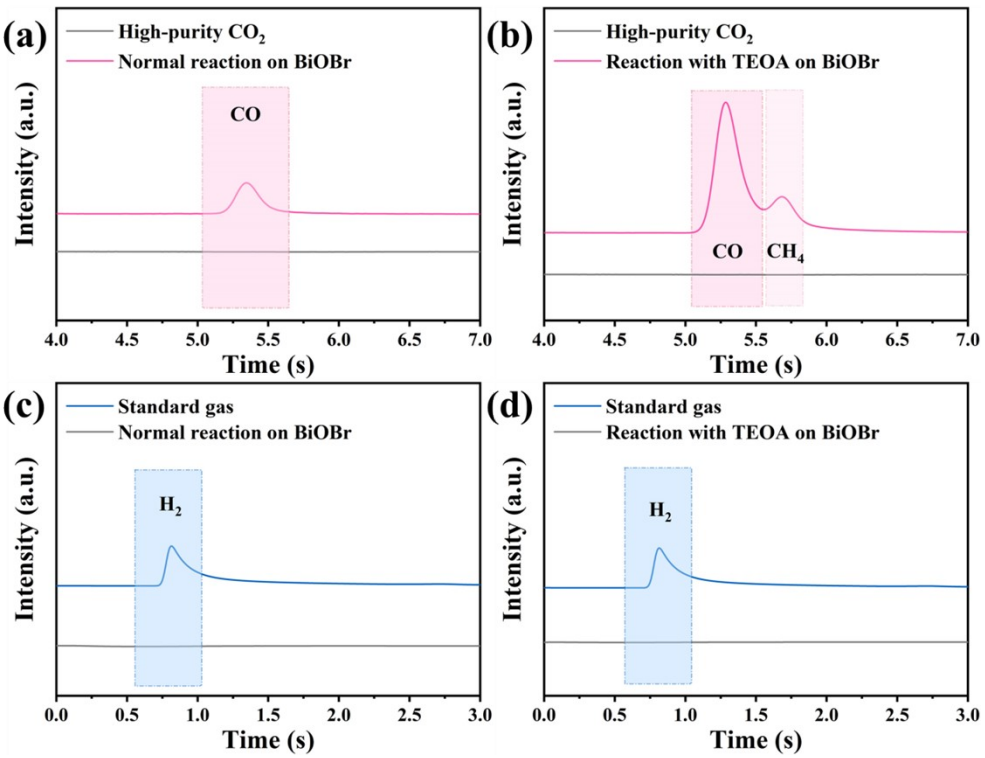

Figure S5. Gas chromatography results of the reaction gases over BiOBr.

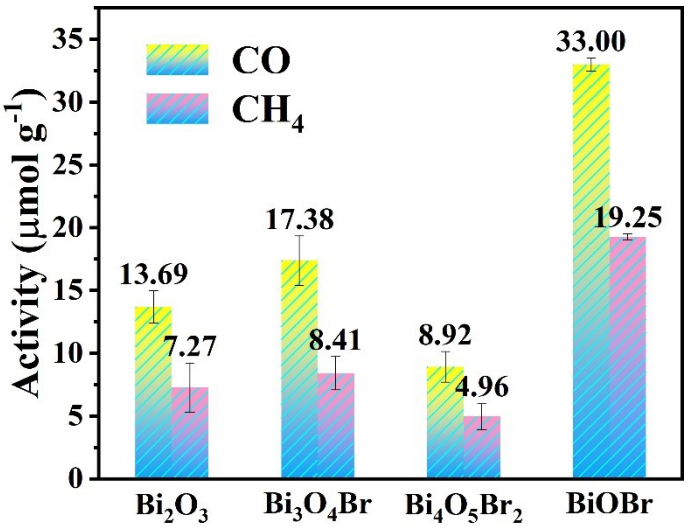

Figure S6 Photocatalytic activity in the presence of TEOA.

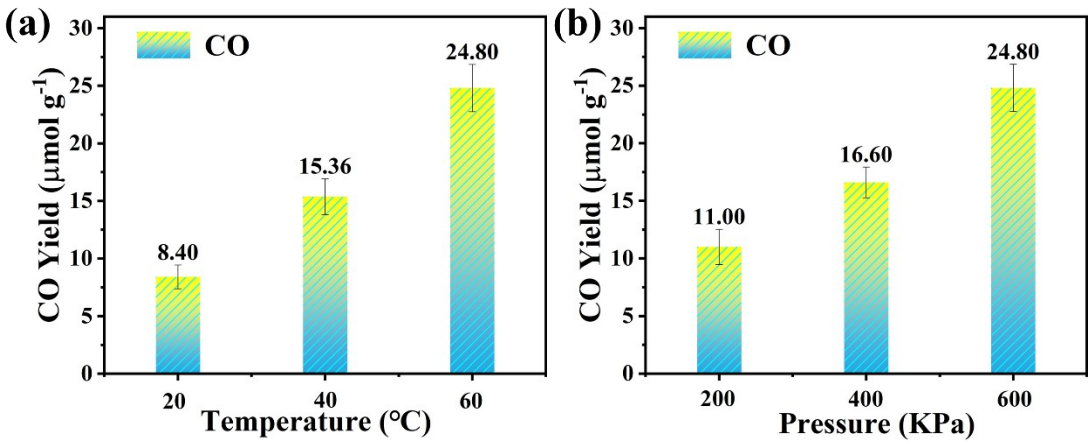

Figure S7. Photocatalytic CO_2 reduction efficiencies of BiOBr at varying (a) temperatures and (b) pressures.

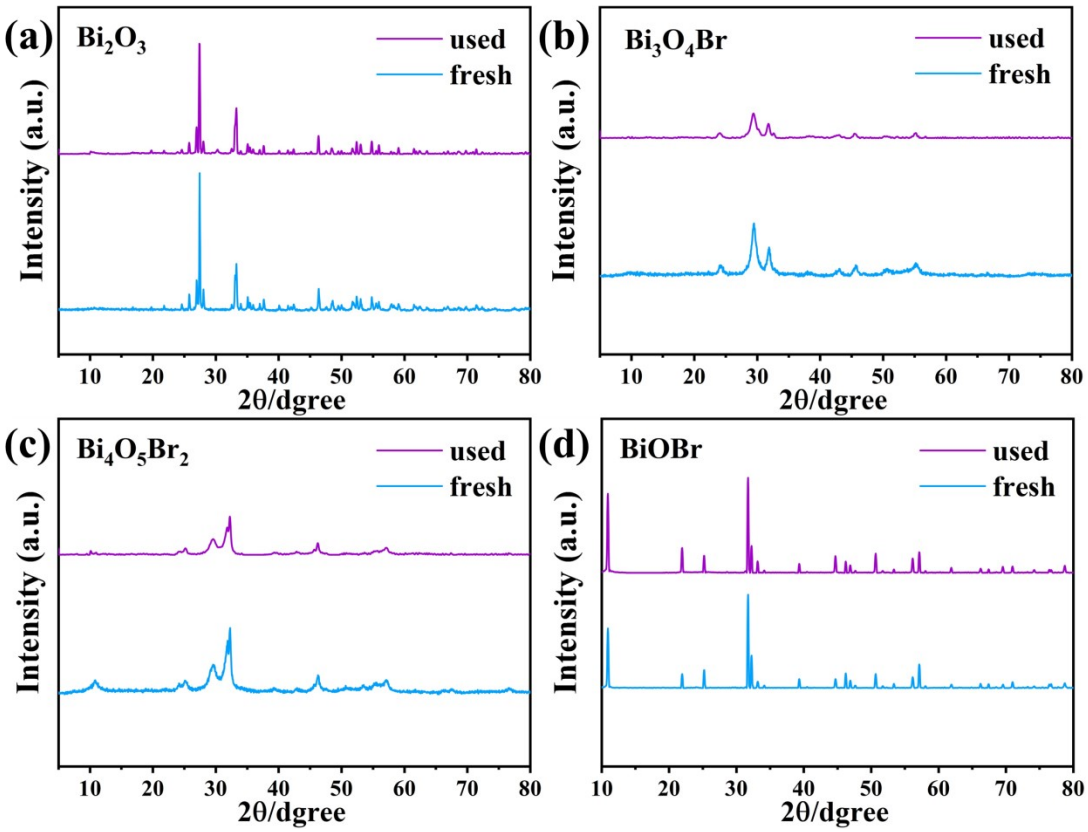

Figure S8. The XRD patterns of (a) Bi_2O_3, (b) Bi_3O_4Br, (c) $Bi_4O_5Br_2$ and (d) BiOBr before and after the photocatalytic tests.

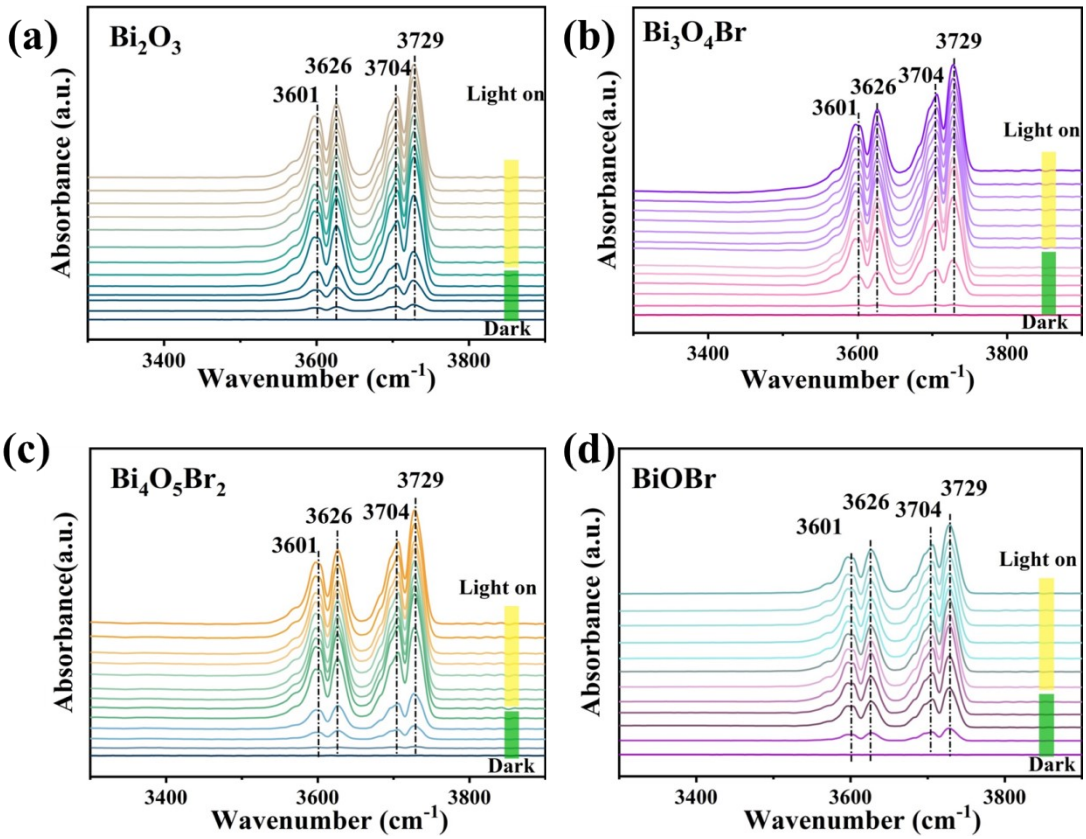

Figure S9. In-situ DRIFTS spectra of (a) Bi_2O_3, (b) Bi_3O_4Br, (c) $Bi_4O_5Br_2$ and (d) BiOBr.

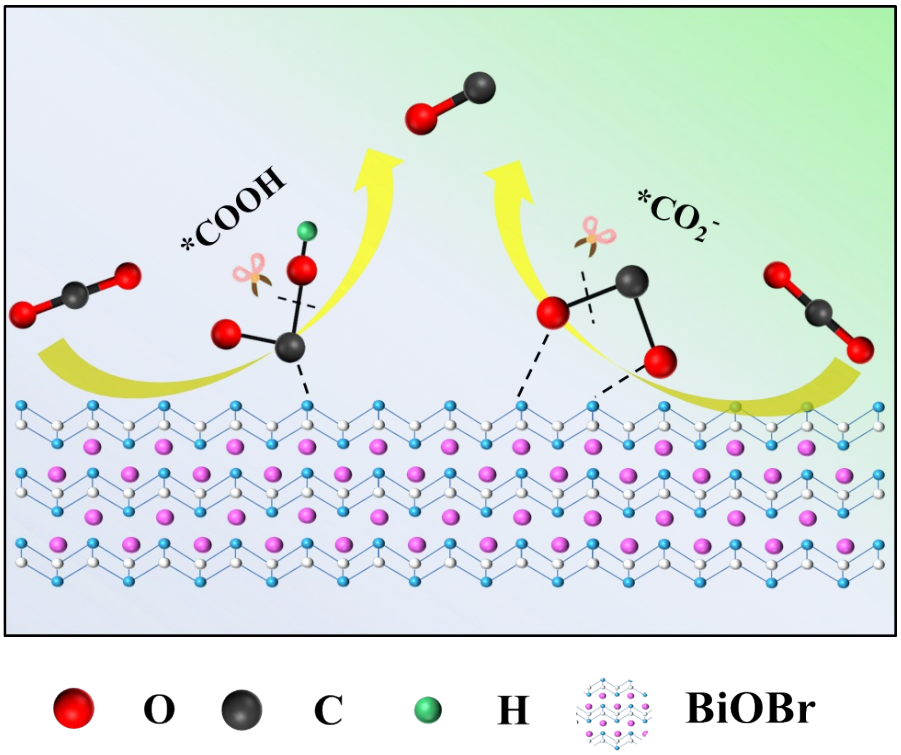

Figure S10. Two possible reaction pathways for the absorbed CO_2 converting to CO over BiOBr.

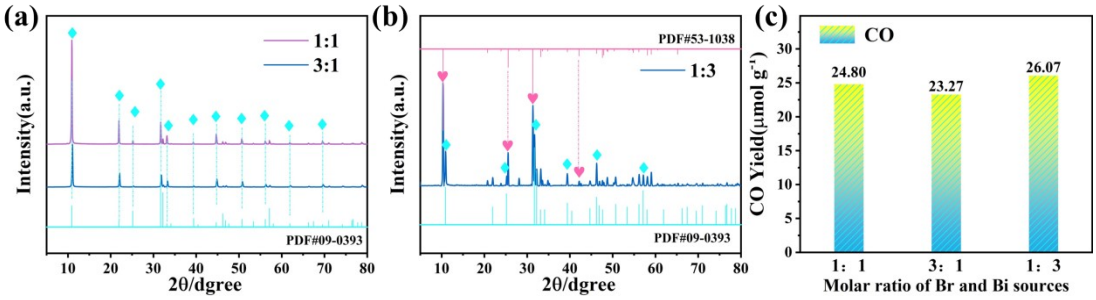

Figure S11. (a, b) XRD patterns and (c) photocatalytic activity comparison for the samples synthesized with different molar ratio of Br and Bi sources.

To modulated the Br content in $Bi_xO_yBr_z$, samples were synthesized following the BiOBr synthesis procedure as depicted in **S1**, by varying molar ratios of KBr: $Bi(NO_3)_3 \cdot 5H_2O$ (3: 1 and 1: 3). With a molar ratio of 3: 1, the XRD pattern (**Figure S11a)** of the as-prepared sample matched the BiOBr standard card PDF#09-0393. Besides, **Figure S11b** revealed the presence of $Bi_6O_6(OH)_3(NO_3)_3 \cdot 1.5H_2O$ (PDF#53-1038) impurities alongside BiOBr when the molar ratio was 1: 3. Moreover, as depicted in **Figure S11c**, the CO activities of the two samples showed only minor variations compared to BiOBr synthesized using the standard method (1:1 ratio). The results above suggested that $Bi_xO_yBr_z$ materials with different Br contents cannot be synthesized by changing the molar ratio of KBr: $Bi(NO_3)_3 \cdot 5H_2O$.

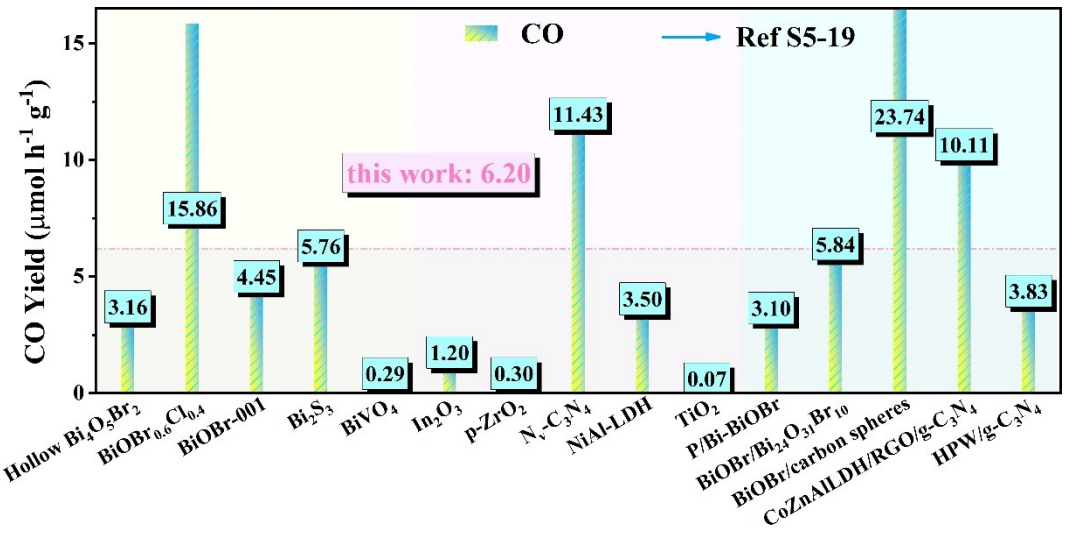

Figure S12. Comparison of the CO yield of BiOBr with those of previously reported works.

Table S1. BET surface area of as-prepared $Bi_xO_yBr_z$ catalysts.

Sample	S_{BET} ($m^2\ g^{-1}$)	Pore Volume ($cm^3\ g^{-1}$)	Pore size (nm)
Bi_3O_4Br	38.12	0.1231	13.20
$Bi_4O_5Br_2$	12.21	0.1000	30.06
BiOBr	2.65	0.0112	20.68

Table S2. Comparison of photocatalysts toward photocatalytic CO_2 reduction.

Catalysts	Main products ($\mu mol\ g^{-1}\ h^{-1}$)	Reaction conditions	Ref.
$BiOBr_{0.6}Cl_{0.4}$	CO: 15.86	H_2O, 300 W Xe lamp	[5]
Hollow $Bi_4O_5Br_2$	CO: 3.16	H_2O, 300 W Xe lamp	[6]
BiOBr-001	CO: 4.45	H_2O, 300 W Xe lamp	[7]
Bi_2S_3	CO: 5.76	H_2O, 300 W Xe lamp	[8]
$BiVO_4$	CO: 0.29	H_2O, 300 W Xe lamp	[9]
In_2O_3	CO: 1.2	H_2O, 300 W Xe lamp	[10]
p-ZrO_2	CO: 0.3	H_2O, 300 W Xe lamp	[11]
TiO_2	CO: 0.07	H_2O, 450 W Xe lamp with a UV filter	[12]
N_v-C_3N_4	CO: 11.43	A 300 W Xe lamp with an AM 1.5 filter	[13]
NiAl-LDH	CO: 3.5	H_2O, 300 W Xe lamp	[14]
P/Bi-BiOBr	CO:3.10	H_2O, 300 W Xe lamp	[15]
$BiOBr/Bi_{24}O_{31}Br_{10}$	CO: 5.84	H_2O, 300 W Xe lamp	[16]
BiOBr/carbon spheres	CO: 23.74	H_2O, 300 W Xe lamp	[17]
CoZnAlLDH/RGO/g-C_3N_4	CO: 10.11	H_2O, 300 W Xe lamp	[18]
HPW/g-C_3N_4	CO: 3.83	H_2O, 500 W Xe lamp	[19]
2D-BiOBr	CO: 6.20	H_2O, 300 W Xe lamp	This work

Reference

[1] L. Zhou, M. Xie, C. Rao, H. Su, Y. Pang, H. Lou, D. Yang and X. Qiu, *Chem. Eng. J.*, 2023, **471**, 144574.

[2] B. Chen, Y. Hou, H. Li, H. Gao, H. Fu, F. Liao, J. Zhang and Y. Liao, *J. Colloid Interface Sci.*, 2023, **652**, 1857-1866.

[3] Z. Long, G. Zhang, H. Du, J. Zhu and J. Li, *J. Hazard. Mater.*, 2021, **407**, 124394.

[4] D. Mao, S. Ding, L. Meng, Y. Dai, C. Sun, S. Yang and H. He, *Appl. Catal. B*, 2017, **207**, 153-165.

[5] M. Gao, J. Yang, T. Sun, Z. Zhang, D. Zhang, H. Huang, H. Lin, Y. Fang and X. Wang, *Appl. Catal. B*, 2019, **243**, 734-740.

[6] X. Jin, C. Lv, X. Zhou, H. Xie, S. Sun, Y. Liu, Q. Meng and G. Chen, *Nano Energy*, 2019, **64**, 103955.

[7] D. Wu, L. Ye, H.Y. Yip and P.K. Wong, *Catal. Sci. Technol.*, 2017, **7**, 265-271.

[8] Z. Miao, Y. Zhang, N. Wang, P. Xu and X. Wang, *J. Colloid Interface Sci.*, 2022, **620**, 407-418.

[9] J. Bian, Z. Zhang, J. Feng, M. Thangamuthu, F. Yang, L. Sun, Z. Li, Y. Qu, D. Tang, Z. Lin, F. Bai, J. Tang and L. Jing, *Angew. Chem. Int. Ed.* 2021, **60**, 20906-20914.

[10] J. Liu, R. Wang, Y. Shang, X. Zou, S. Wu and Q. Zhong, *J. Colloid Interface Sci.*, 2024, **663**, 21-30.

[11] X. Xiong, C. Mao, Z. Yang, Q. Zhang, G. I. N. Waterhouse, L. Gu and T. Zhang, *Adv. Energy Mater.*, 2020, **10**, 2002928.

[12] C. Zhao, L. Liu, G. Rao, H. Zhao, L. Wang, J. Xu and Y. Li, *Catal. Sci. Technol.*, 2015, **5**, 3288-3295.

[13] Y. Wang, C. Ban, Y. Feng, J. Ma, J. Ding, X. Wang, L. Ruan, Y. Duan, M. G. Brik, L. Gan and X. Zhou, *Nano Energy*, 2024, **124**, 109494.

[14] R. N. Wang, Z. Y. Qiu, S. P. Wan, Y. N. Wang, Q. Liu, J. Ding and Q. Zhong, *Chem. Eng. J.*, 2022, **427**, 130863.

[15] J. Zhu, Y. Li, X. Wang, J. Zhao, Y. Wu and F. Li, *ACS Sustain. Chem. Eng.*, 2019, **7**, 14953-14961.

[16] Y. Feng, J. Xie, Z. Lu, A. Hao, J. Hu and Y. Cao, *J. Nanopart. Res.*, 2022, **24**, 27.

[17] K. Liu, X. Zhang, C. Zhang, G. Ren, Z. Zheng, Z. Lv and C. Fan, *RSC Adv.*, 2019, **9**, 14391-14399.

[18] Y. Yang, J. Wu, T. Xiao, Z. Tang, J. Shen, H. Li, Y. Zhou and Z. Zou, *Appl. Catal. B,* 2019, **255**, 117771.

[19] X. Jiang, Z. Zhang, M. Sun, W. Liu, J. Huang and H. Xu, *Appl. Catal. B*, 2021, **281**, 119473.